Transient Relativistic Plasma Grating to Tailor High-Power Laser Fields, Wakefield Plasma Waves, and Electron Injection

Transient Relativistic Plasma Grating to Tailor High-Power Laser Fields, Wakefield Plasma Waves, and Electron Injection

Qiang Chen,[1] Dominika Maslarova,[2,3] Junzhi Wang,[1] Shao Xian Lee,[1] Vojtech Horný,[4,5] and Donald Umstadter[1,*]

[1]Extreme Light Laboratory, Department of Physics and Astronomy, University of Nebraska-Lincoln, Lincoln, Nebraska 68588, USA

[2]Institute of Plasma Physics of the Czech Academy of Sciences, Za Slovankou 1782/3, 182 00 Prague, Czech Republic

[3]Faculty of Nuclear Sciences and Physical Engineering, Czech Technical University in Prague, Břehová 78/7, 115 19 Prague, Czech Republic

[4]Department of Physics, Chalmers University of Technology, Fysikgarden 1, 412 58 Gothenburg, Sweden

[5]LULI-CNRS, École Polytechnique, CEA: Université Paris-Saclay; UPMC Univ Paris 06: Sorbonne Universités, F-91128 Palaiseau Cedex, France

(Received 12 July 2021; revised 20 January 2022; accepted 21 March 2022; published 20 April 2022)

We show the first experiment of a transverse laser interference for electron injection into the laser plasma accelerators. Simulations show such an injection is different from previous methods, as electrons are trapped into later acceleration buckets other than the leading ones. With optimal plasma tapering, the dephasing limit of such unprecedented electron beams could be potentially increased by an order of magnitude. In simulations, the interference drives a relativistic plasma grating, which triggers the splitting of relativistic-intensity laser pulses and wakefield. Consequently, spatially dual electron beams are accelerated, as also confirmed by the experiment.

DOI: 10.1103/PhysRevLett.128.164801

An intense, ultrashort laser pulse can drive a large-amplitude plasma wave [1–4], which has been shown in laboratory studies to accelerate electrons [5–7] to multi-GeV energy over only centimeter-scale distance [8–10]. Such compact laser plasma accelerators (LPAs) are suitable for seeding a free-electron laser [11], Thomson x-ray sources [12,13], and future compact TeV electron-positron colliders [14].

Prior to being trapped in and accelerated by a laser wakefield, electrons need to be preaccelerated to catch up with the wakefield with a proper velocity and at the proper phase, which is called injection process. Among several controlled injection methods, the optical injection [15–22] relies on the ponderomotive force [23] of the laser field on electrons $F_p \simeq -(1/\gamma)\nabla a^2/2$, where γ is the Lorentz factor of the electron, $a = 0.855\lambda[\mu\mathrm{m}](I[\times 10^{18}\ \mathrm{W/cm^2}])^{1/2}$ is the normalized vector potential of the laser pulse, λ is the laser wavelength, and I is the laser intensity. As originally proposed, an intense ($a > 1$) laser pulse (injector) can directly inject electrons into the wakefield of another laser pulse (driver) [15]. Later, it was suggested to replace the single intense injector pulse with two much weaker ($a_1 = a_2 = 0.2$), colliding laser pulses [16], whose beat wave, however, gives a large ponderomotive force (due to a smaller intensity gradient scale length) and therefore allows more efficient electron preacceleration and injection.

This beat wave assisted injection has been demonstrated [18–22], although the original three-beam scheme [16] was simplified to a two-beam case (colliding pulse injection, CPI), where one driver overlaps with one identically polarized injector to form a beat wave [17]. Experimentally, the beat wave has always been aligned approximately parallel to the driver and wakefield propagation direction ($\theta \sim 180°$, with $\theta = 0°$ for collinear and $\theta = 180°$ for counterpropagating geometries) to efficiently "kick" electrons to a relativistic velocity to catch up with the wakefield. If the beat wave approaches perpendicular to the wakefield (nearly collinear geometry, $\theta \sim 0°$), it cannot push the electrons longitudinally to catch up with the wakefield [17]. Within the scarce optical injection experiments [18–22], the smallest intersection angle for CPI used was $\theta = 135°$ [20,22]. A further reduction in the collision angle has never been tested, as believed inefficient for preacceleration of electrons in the wakefield propagation direction [17]. However, recent results and analysis of 2D simulations of noncollinear CPI have indicated that injection by two intersecting pulses is multidimensional (involving not only longitudinal, but also transverse movements of electrons with respect to the wakefield propagation) [24]. Here, for the first time, we show that the deviation from the counterpropagating geometry can be the main cause of the consequent electron trapping.

In the experiment (see Fig. 1), the Diocles laser was split into two similar laser pulses (wavelength $\lambda_0 = 800$ nm, duration $\tau_1 = 39$ fs, $\tau_2 = 35$ fs), with each focused to high intensity [$f/14$; with intensity full width at half maximum

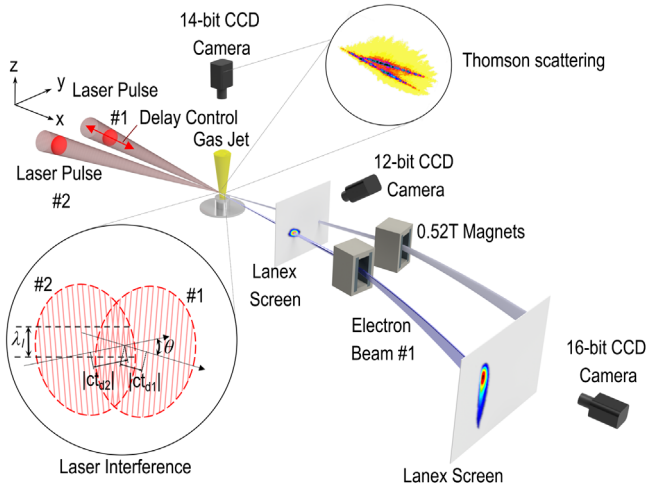

FIG. 1. Experiment setup for the electron injection and acceleration. The left-bottom inset illustrates, from the top view, the formation of the interference with a wavelength $\lambda_I = \lambda_0/[2\sin(\theta/2)] = 4.6\ \mu$m.

(FWHM) $\sim 18\ \mu$m; $a_1 = 1.37$, $a_2 = 1.52$] near the entrance of a gas jet with 2-mm-diameter circular orifice. While the crossing angle of two laser pulses was fixed at $\theta = 10°$, their relative temporal delay $\tau_d = t_{d1} - t_{d2}$ ($t_{d1,2}$ for the respective laser pulses' arrival time to the collision point) was adjustable by a motorized stage to an accuracy of 0.2 μm. The spatial profile of the accelerated electron beams was diagnosed by a fluorescent screen imaged by a CCD camera. The electron beam spectrum was measured by a dipole-magnet spectrometer, with a resolution 5% for energy range 30–150 MeV (neglecting finite beam divergence).

In Fig. 2, we present both experimental and numerical results of the injection induced by the interference. The gas density was reduced below certain thresholds so that injection was suppressed for individual wakefields. Figures 2(a) and 2(b), respectively, show a typical experimentally measured profile and spectrum of the trapped and accelerated electron beam. The averaged density of gas (99% helium and 1% nitrogen) was measured offline and is equivalent to a plasma density $n_e \approx 5 \times 10^{18}$ cm^{-3}. The optimized accelerated electron beam has a charge of $\sim$4 pC and a transverse divergence angle of 4.2×4.5 mrad^2, which are comparable to the previous results of injection obtained with counterpropagating pulses [18–22]. The spectrum has a central energy of 110 MeV and an energy spread of 70 MeV (FWHM).

To explore the underlying physics, particle-in-cell (PIC) simulations were performed with the SMILEI code [25]. In this short Letter, we present results from the simple 2D simulations with helium to explain the major physics, and the corroborations from 3D simulation were included in the Supplemental Material [26]. The simulation box range was $[0\ \mu\text{m}, 796\ \mu\text{m}]$ in the x direction and $[0\ \mu\text{m}, 232\ \mu\text{m}]$ in the y direction. Each cell had a size of $\Delta x \times \Delta y = 0.033 \times 0.05\ \mu$m^2 and included two helium macroparticles. The initial density profile of neutral helium started with a 50-μm-long linear density up-ramp in the x direction, followed by 746-μm-long plateau of 2.5×10^{18} cm^{-3}. Two spatiotemporally Gaussian laser beams moving, respectively, at a $-5°$ and 5° angle from the x axis were

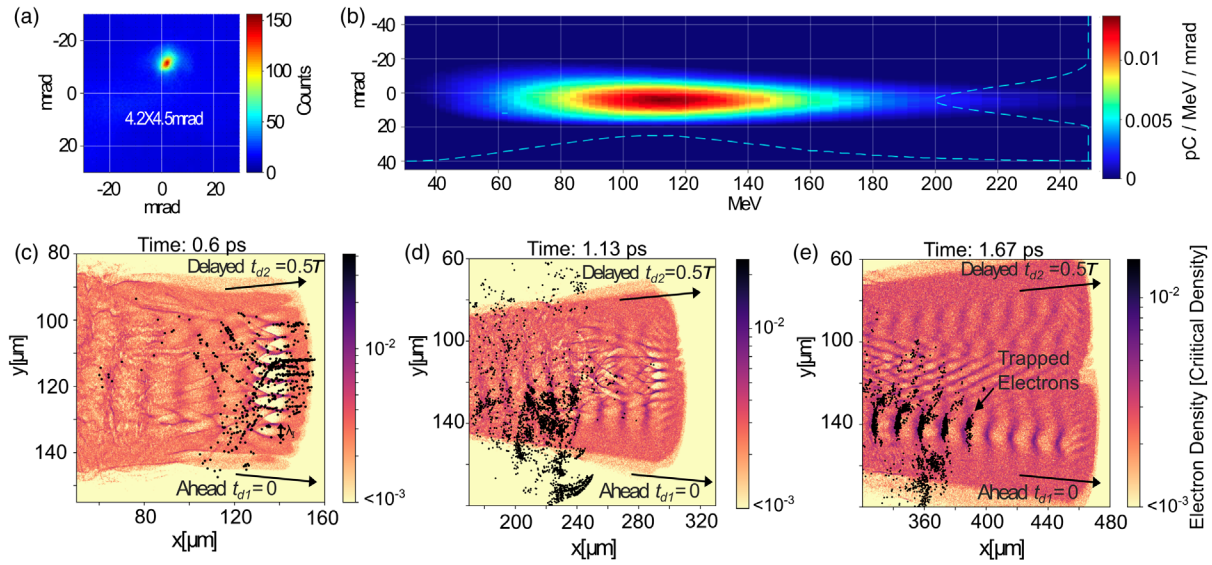

FIG. 2. Electron beam injection and trapping process. (a) Experiment: spatial profile of the electron beam measured in the direction of laser beam 1, with an average plasma density $n_e \approx 5 \times 10^{18}$ cm^{-3} corresponding to full gas ionization. (b) Experiment: electron beam spectrum of (a). (c)–(e) Simulation: electron density profile in the simulation time of 0.6 ps [(c) laser-laser overlap], 1.13 ps [(d) wakefield recovering], and 1.67 ps [(e) electron trapping]. One beam arrived at the intersection at $t_{d1} = 0$, while the other delayed one arrived at $t_{d2} = 0.5\tau$. Black dots correspond to electron macroparticles that were injected.

both focused to $(x, y) = (116\ \mu\text{m}, 116\ \mu\text{m})$. The laser parameters were identical to each other and similar to those in the experiment: wavelength $\lambda_0 = 0.8\ \mu$m, normalized vector potential $a_0 = 1.3$, FWHM beam diameter 18 μm (waist $w_0 = 14\ \mu$m), FWHM duration $\tau = 29$ fs, and p polarized in the x-y plane. Upon each ionization event, a new electron macroparticle was created, calculated by a Monte Carlo module for tunneling ionization.

Figures 2(c)–2(e) show the PIC simulation results. First, when two laser pulses both arrive at the common focus region at time 0.6 ps [Fig. 2(c)], their interference $[\lambda_I = \lambda_0/[2\sin(\theta/2)] = 4.6\ \mu\text{m}]$ forms a periodic ponderomotive force which drives a transient electron density grating. At this stage, the electrons are channeled and multidimensionally accelerated by the interference [29]. Second, when the pulses have already moved away from each other at time 1.13 ps [Fig. 2(d)], the interference subsides, and the electrons will no longer be trapped by the interference. Instead, they move into a complex region of the dual-beam-driven wakefield. Last, when the pulses have departed far away enough from each other at time 1.67 ps [Fig. 2(e)], the wakefield following the leading laser pulse is almost recovered. Novel trapping of the electrons which were previously dephased occurs in the fifth to eighth bubbles. Note that the delayed pulse's wakefield traps almost no electrons, which will be discussed later.

All the main injection features, such as multibucket trapping, wakefield, and beam splitting, and the driver or injector switch were preserved in 3D simulations with pure helium. In the test simulations with mixture (99% helium and 1% nitrogen, as in experiment), among the injected electrons, the ionized electrons from the nitrogen are only a few percent. In addition, those electrons are exposed to the interference upon ionization; thus, they do not differ from other majority electrons from the colliding pulse injection. The same physics would apply to LPA with other gases, such as hydrogen, which is preferable to generate plasma channels for LPA.

Corresponding to Figs. 2(c)–2(e), the evolution of the electron energy during the injection process is shown in Fig. 3. In the interference pattern, electrons experience the transverse standing wave and a traveling wave propagating in the x direction [30]. While the electrons are pushed to the nodes of the standing wave [29,31], they oscillate in the electric field of the traveling wave and gain energy up to $\gamma_{\max} \sim 4$. The oscillations then gradually abate when electrons see the falling edge of the interference, reaching the minimum energy when the pulses separate transversely by $\sim w_0$. Subsequently, the electrons started accelerating in the forming wakefields. They gradually form compact electron bunches in one wakefield as two wakefields separate from each other. Only the electrons which are originally channeled to the nodes of the standing wave are eventually trapped in the wakefield. Therefore, the role of the plasma grating is essential in the injection process, as it dephases the electrons to the fields of the plasma waves.

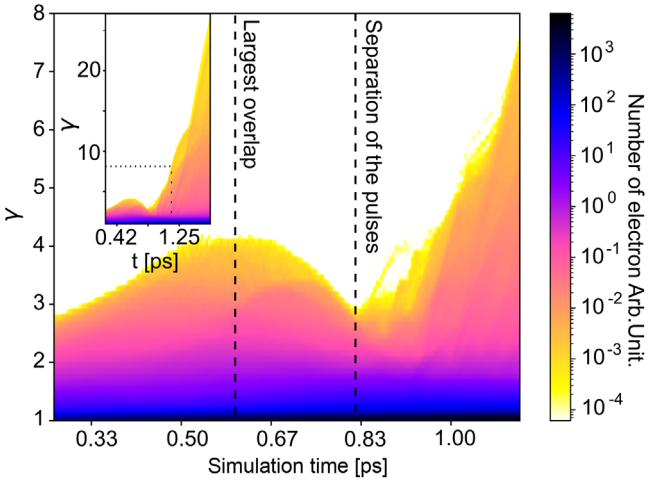

FIG. 3. Energy evolution of plasma electrons during the injection process shown in Fig. 2. The dashed lines show the times of the largest overlap of the laser beams and the time when the laser beams transversely separate by w_0 at the simulation times of 0.6 and 0.82 ps, respectively. The inset shows further energy evolution [until Fig. 2(e) stage]; the dotted rectangle part corresponds to the main figure.

Both laser pulses can play the role of either the wakefield driver or electron injector, depending on their relative delay τ_d on arriving at the collision point. Figure 4(a) shows the charges $Q_{1,2}$ of the respective accelerated electron beams in the direction of either laser pulse, as a function of the delay τ_d, in the unit of FWHM pulse duration $\tau_0 = \tau_2 = 35$ fs. Overall, the injection only occurs within the pulse overlap range taken to be where the E-field envelope is at $1/e^2$ of the maximum, or approximately $4\tau_0$. It is possible to inject electrons into both wakefields (more details will be presented in another upcoming work), while, more generally, as the delay increases, the direction of the accelerated electrons switches from following pulse 1 ($\tau_d < 0$) to pulse 2 ($\tau_d > 0$), indicating that the role of the injector or driver played by each pulse has switched, and the electrons were more likely to be pushed by the delayed injector into the wakefield of the leading laser pulse. The injection following pulse 1 with charge $Q_1(\tau_d)$ is not "symmetric" or "identical" to that following pulse 2 with charge $Q_2(\tau_d)$, mainly because of the differences in the two laser pulses' peak intensities and durations.

The dependence of the amount of injected charge Q_2 on pulse delay τ_d was also examined in Fig. 4(b) (see the Supplemental Material [26] for 3D results which show the same trend here). Note, $Q_1(\tau_d) = Q_2(-\tau_d)$ due to the symmetry. The respective amplitudes of the interference A_i (theoretical calculation) and the wakefield A_w (simulations) versus delay τ_d were also plotted. Charge Q_2 was found the highest with delays between 1.5τ ($\tau = 29$ fs is the FWHM pulse duration) and 2τ, and the lowest with delays between

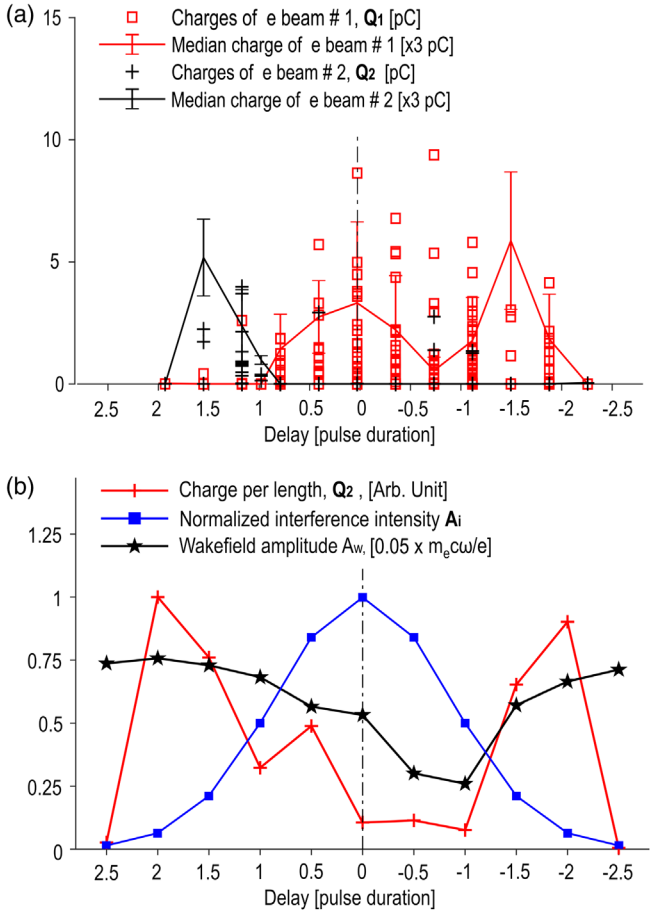

FIG. 4. Dependence of electron injection on pulse delay. (a) Experiment: charge of the optically injected electron beam (s) $Q_{1,2}$, their statistical medians, and median absolute deviation, in either laser pulse direction, as a function of delay τ_d, with units in the pulse duration $\tau_0 = 35$ fs. Positive τ_d means pulse 2 ahead and negative for pulse 1 ahead. (b) Simulation: delay scan with units in the pulse duration $\tau = 29$ fs to see changes in the injected charge per length Q_2 (red, considering electrons whose energy reached ≥ 15 MeV in the time of 2.70 ps), the maximum wakefield amplitude A_w (black, for recovered wakefields at 1.49 ps), and the maximum interference intensity A_i (blue).

0τ and 1τ. The latter case of almost exact overlap and strong interference ($A_i/A_i^{\max} \sim 100\%$), however, results in deeply modulated electron density grating, which distorted the laser pulse and therefore deteriorated the wakefield to an amplitude $A_w/A_w^{\max} \sim 10\%$. The low-quality and weak plasma wave was unable to trap a significant number of electrons. Note that in the simulations of pulses with polarizations perpendicular to each other, in which case, interference cannot occur, neither electron injection nor splitting of laser pulses or wakefields was observed.

In the cases of the long exposures of electrons to the strong interference (τ_d between 0τ and 1τ), the imprint of the electron density grating on the laser pulse and its wakefield persists throughout electron acceleration, such as shown in Fig. 5(a). The simulation result of split electron beams was also observed in tens of shots in the experiment, such as shown in Fig. 5(b). Each of the two electron beams follows laser beam 2 and has a divergence angle of $\delta\theta_{y,z} \sim 4$ mrad, and they are separated from each other by an angle of $\Delta\theta_y \sim 10$ mrad. Multiple split patterns for the dual electron beams were observed in experiment, such as shown in Fig. 5(c), which manifested asymmetric wakefields or radial forces perpendicular to the laser propagation. This might be due to the imperfect overlap of two laser pulses in the z direction, as a result of the shot-to-shot pointing jitters of laser pulses near the level of a beam size. The indications of the laser pulse splitting were also observed; however, the results are not provable enough to make conclusive statements at this point.

In summary, we experimentally demonstrated the injection of an electron beam and dual electron beams into laser wakefield plasma waves, using intense, nearly collinear, and interfering laser pulses. The role of the laser pulse overlap is quantitatively examined by scanning the relative delay of two laser pulses on arriving at their collision point. The simulation results agreed with the experimental observations of electron beam splitting and the overlap-dependent injection features. Those characteristics are a result of the interference-driven electron plasma grating, which modulates, in turn, the laser pulses and plasma waves

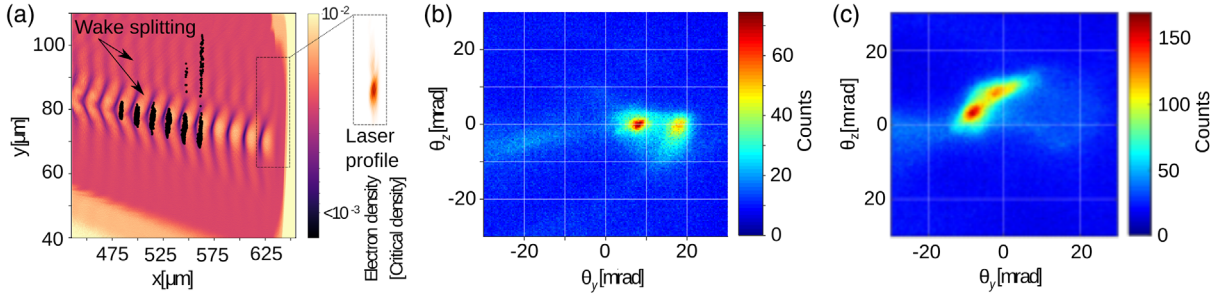

FIG. 5. Nearly parallel electron beams simultaneously accelerated by a modulated wakefield. (a) Simulation: electron density profile showing wakefield splitting $\Delta x \approx 510$ μm after the injection process depicted in Fig. 2. Black dots represent examples of trapped electron macroparticles. The inset shows the corresponding modulated laser intensity profile (in arb. units). (b),(c) Experiment: electron spatial profile showing dual electron beams split along different directions.

driven by them. Our Letter is fundamental to a proper understanding of the colliding pulse injection. Our Letter is also the first evidence of a relativistic, transient electron grating for manipulation of relativistic-intensity light, plasma waves, and electron beams. This might highlight a road from intense plasma optics [32–36] to relativistic plasma optics. Moreover, instead of injecting electrons into the leading bucket like other injection schemes, our scheme enables sole trapping into later buckets in lower-density plasma. Such an injection triggered in the weakly nonlinear regime allows for its combination with the method of optimal plasma density tapering [37–41], which opens further potential of increasing the dephasing limit. By optimally tapering the plasma density, the electron beam injected into the Nth bucket behind the laser can be locked with the maximum acceleration phase for longer distance and accelerated to higher peak energy: $\Delta\gamma_N^{\max}/\Delta\gamma_{\hom} \approx 2^{-3/2} \exp(1/2)\omega_{p0}\tau_0|\Phi_N| \approx |\Phi_N| \approx \pi(2N-1)$, where $\Delta\gamma_{\hom}$ is the energy gain without plasma tapering (homogeneous density), ω_{p0} is the initial plasma frequency, τ_0 is the initial laser pulse duration (use typical $\omega_{p0}\tau_0 \sim \sqrt{2}$), and Φ_N is the maximum acceleration phase in the Nth bucket of the wakefield [38–41]. With $N = 5$ demonstrated by our scheme, the increase of the dephasing limit is approximately $\Delta\gamma_N^{\max}/\Delta\gamma_{\hom} \approx \pi(2N-1) \approx 30$, accelerated in a tapering length of $\sim(2N-1) = 9\times$ dephasing length ($L_d \approx \lambda_p^3/2\lambda_0^2 \approx 2.5$ mm for $n_e \approx 5\times 10^{18}$ cm^{-3}). Note the previous colliding pulse injection schemes [18–22] also work in the weakly nonlinear regime and could combine with optimal plasma tapering corresponding to $N = 1$, thus, a potential energy gain of $\sim$3.

As an example, a 3D tailored plasma channel [41,42] can be applied for the optimal tapering. Inside the tailored plasma channel, the driver laser naturally diffracts for about a few Rayleigh lengths and then gets guided by a plasma lens and a plasma waveguide. This process slightly decreases the laser intensity to $a_0 \sim 0.5$; thus, it helps increase the pump depletion length ($L_{pd}/L_d \approx 2\omega_{p0}\tau_0/a_0^2 \approx$ 11.2) to surpass the above-mentioned tapering length. The transverse expansion of the electron beam is negligible, therefore allowing for further LPA process [42], namely, the optimal tapering for our case [41]. The final energy of the electron beam is estimated to be $\Delta W \approx 30 \times \Delta W_{\hom} \approx$ 4.1 GeV, based on the $\sim$20 TW laser and $\sim$2 cm acceleration length, where $\Delta W_{\hom} \approx 0.630 I(\mathrm{Wcm}^{-2})/n_e(\mathrm{cm}^{-3}) \approx$ 0.137 GeV [23] is the energy gain without tapering.

This work is supported by the U.S. Department of Energy, Office of Science, High Energy Physics under Award No. DE-SC0019421. Travel support was provided by the University of Nebraska-Lincoln College of Arts and Sciences International Research Collaboration Award. This work was supported by the Ministry of Education, Youth and Sports of the Czech Republic through the e-INFRA CZ (ID: 90140). This work is also supported by European Regional Development Fund-Project "Center for Advanced Applied Science" (No. CZ.02.1.01/0.0/0.0/16_019/0000778) and Student Grant Competition of CTU (No. SGS22/185/OHK4/3T/14). This project has received funding from the European Research Council under the European Union's Horizon 2020 research and innovation program under Grants Agreement No. 647121 and No. 787539. The authors would like to thank Dr. Jan Psikal and Dr. Miroslav Krus for fruitful discussions on the topic. Additional support was provided by the U.S. Department of Energy, Office of Science, Fusion Energy Sciences, Award No. DE-SC0021018; LaserNetUS initiative at the Extreme Light Laboratory; the U.S. Army Research Office Award No. W911NF-17-2-0178.

*donald.umstadter@unl.edu

[1] T. Tajima and J. M. Dawson, Phys. Rev. Lett. **43**, 267 (1979).
[2] P. Sprangle, E. Esarey, A. Ting, and G. Joyce, Appl. Phys. Lett. **53**, 2146 (1988).
[3] A. Modena, Z. Najmudin, A. E. Dangor, C. E. Clayton, K. A. Marsh, C. Joshi, V. Malka, C. B. Darrow, C. Danson, D. Neely, and F. N. Walsh, Nature (London) **377**, 606 (1995).
[4] D. Umstadter, S. Y. Chen, A. Maksimchuk, G. Mourou, and R. Wagner, Science **273**, 472 (1996).
[5] J. Faure, Y. Glinec, A. Pukhov, and S. Kiselev, Nature (London) **431**, 541 (2004).
[6] S. P. D. Mangles, C. D. Murphy, Z. Najmudin *et al.*, Nature (London) **431**, 535 (2004).
[7] C. G. R. Geddes, C. S. Toth, J. van Tilborg, E. Esarey, C. B. Schroeder, D. Bruhwiler, C. Nieter, J. Cary, and W. P. Leemans, Nature (London) **431**, 538 (2004).
[8] A. J. Gonsalves, K. Nakamura, J. Daniels, C. Benedetti, C. Pieroneke*t al.*, Phys. Rev. Lett. **122**, 084801 (2019).
[9] W. P. Leemans, B. Nagler, A. J. Gonsalves, C. Tóth, K. Nakamura, C. G. Geddes, E. Esarey, C. B. Schroeder, and S. M. Hooker, Nat. Phys. **2**, 696 (2006).
[10] M. Litos, E. Adli, W. An *et al.*, Nature (London) **515**, 92 (2014).
[11] M. Fuchs, R. Weingartner, A. Popp *et al.*, Nat. Phys. **5**, 826 (2009).
[12] J. M. Cole, K. T. Behm, E. Gerstmayr, T. G. Blackburn, J. C. Wood *et al.*, Phys. Rev. X **8**, 011020 (2018).,
[13] K. Poder, M. Tamburini, G. Sarri, A. DiPiazza, S. Kuschel *et al.*, Phys. Rev. X **8**, 031004 (2018).
[14] K. Nakajima, J. Wheeler, G. Mourou, and T. Tajima, Int. J. Mod. Phys. A **34**, 1943003 (2019).
[15] D. Umstadter, J. K. Kim, and E. Dodd, Phys. Rev. Lett. **76**, 2073 (1996).
[16] E. Esarey, R. F. Hubbard, W. P. Leemans, A. Ting, and P. Sprangle, Phys. Rev. Lett. **79**, 2682 (1997).
[17] G. Fubiani, E. Esarey, C. B. Schroeder, and W. P. Leemans, Phys. Rev. E **70**, 016402 (2004).
[18] J. Faure, C. Rechatin, A. Norlin, A. Lifschitz, Y. Glinec, and V. Malka, Nature (London) **444**, 737 (2006).

[19] J. Faure, C. Rechatin, A. Norlin, F. Burgy, A. Tafzi, J. Rousseau, and V. Malka, Plasma Phys. Control. Fusion **49**, B395 (2007).
[20] H. Kotaki, I. Daito, M. Kando, Y. Hayashi, K. Kawase*et al.*, Phys. Rev. Lett. **103**, 194803 (2009).
[21] C. Rechatin, J. Faure, A. Ben-Ismaïl, J. Lim, R. Fitour, A. Specka, H. Videau, A. Tafzi, F. Burgy, and V. Malka, Phys. Rev. Lett. **102**, 164801 (2009).
[22] S. Corde, K. T. Phuoc, R. Fitour, J. Faure, A. Tafzi, J. P. Goddet, V. Malka, and A. Rousse, Phys. Rev. Lett. **107**, 255003 (2011).
[23] E. Esarey, C. B. Schroeder, and W. P. Leemans, Rev. Mod. Phys. **81**, 1229 (2009).
[24] G. Golovin, W. Yan, J. Luo, C. Fruhling, D. Haden, B. Zhao, C. Liu, M. Chen, S. Chen, P. Zhang, S. Banerjee, and D. Umstadter, Phys. Rev. Lett. **121**, 104801 (2018).
[25] J. Derouillat, A. Beck, F. Pérez, T. Vinci, M. Chiaramello, A. Grassi, M. Flé, G. Bouchard, I. Plotnikov, and N. Aunai, Comput. Phys. Commun. **222**, 351 (2018).
[26] See Supplemental Material http://link.aps.org/supplemental/10.1103/PhysRevLett.128.164801 for several other aspects of the optical injection process which are out of the scope of the main Letter, which includes Refs. [27,28].
[27] F. S. Tsung, W. Lu, M. Tzoufras, W. B. Mori, C. Joshi, J. M. Vieira, L. O. Silva, and R. A. Fonseca, Phys. Plasmas **13**, 056708 (2006).
[28] A. Pukhov and J. Meyer-ter-Vehn, Appl. Phys. B **74**, 355 (2002).
[29] Z.-M. Sheng, K. Mima, Y. Sentoku, M. S. Jovanović, T. Taguchi, J. Zhang, and J. Meyerter-Vehn, Phys. Rev. Lett. **88**, 055004 (2002).
[30] D. Mašlárová, V. Horný, Q. Chen, J. Wang, S. X. Li, and D. Umstadter, Proc. SPIE Int. Soc. Opt. Eng. **11779**, 1177907 (2021).
[31] D. Bauer, P. Mulser, and W.-H. Steeb, Phys. Rev. Lett. **75**, 4622 (1995).
[32] V. A. Bushuev, B. I. Mantsyzov, and A. A. Skorynin, Phys. Rev. A **79**, 053811 (2009).
[33] S. E. Svyakhovskiy, V. O. Kompanets, A. I. Maydykovskiy, T. V. Murzina, S. V. Chekalin, A. A. Skorynin, V. A. Bushuev, and B. I. Mantsyzov, Phys. Rev. A **86**, 013843 (2012).
[34] P. Michel, E. Kur, M. Lazarow, T. Chapman, L. Divol, and J. S. Wurtele, Phys. Rev. X **10**, 021039 (2020).
[35] A. Leblanc, A. Denoeud, L. Chopineau, G. Mennerat, P. Martin, and F. Quéré, Nat. Phys. **13**, 440 (2017).
[36] G. Lehmann and K. H. Spatschek, Phys. Plasmas **26**, 013106 (2019).
[37] T. Katsouleas, Phys. Rev. A **33**, 2056 (1986).
[38] V. Bulanov, V. A. Vshivkov, G. I. Dudnikova, N. M. Naumova, F. Pegoraro, and I. V. Pogorelsky, Plasma Phys. Rep. **23**, 259 (1997).
[39] A. Pukhov and I. Kostyukov, Phys. Rev. E **77**, 025401(R) (2008).
[40] P. Sprangle, B. Hafizi, J. R. Peñano, R. F. Hubbard, A. Ting, C. I. Moore, D. F. Gordon, A. Zigler, D. Kaganovich, and T. M. Antonsen, Jr., Phys. Rev. E **63**, 056405 (2001).
[41] W. Rittershofer, C. B. Schroeder, E. Esarey, F. J. Grüner, and W. P. Leemans, Phys. Plasmas **17**, 063104 (2010).
[42] D. P. Grote, A. Friedman, C. G. R. Geddes, R. Lehe, C. Benedetti, T. M. Ostermayr, H.-E. Tsai, J.-L. Vay, C. B. Schroeder, and E. Esarey, Phys. Plasmas **28**, 123104 (2021).